Structures, stabilities, and magnetic properties of the Fe_nAu ($n = 1$–12) clusters*

Jin Lv(吕瑾)†, Jiang-Yan Zhang(张江燕), Rui-Rui Liang(梁瑞瑞), and Hai-Shun Wu(武海顺)

School of Chemistry and Material Science, Shanxi Normal University, Linfen 041004, *China*

(Received 24 January 2016; revised manuscript received 2 April 2016; published online 25 May 2016)

The configurations, stabilities, electronic, and magnetic properties of Fe_nAu ($n = 1$–12) clusters are investigated systematically by using the relativistic all-electron density functional theory with the generalized gradient approximation. The substitutional effects of Au in Fe_{n+1} ($n = 1$, 2, 4, 5, 10–12) clusters are found in optimized structures which keep the similar frameworks with the most stable Fe_{n+1} clusters. And the growth way for Fe_nAu ($n = 6$–9) clusters is that the Au atom occupies a peripheral position of Fe_n cluster. The peaks appear respectively at $n = 6$ and 9 for Fe_nAu clusters and at $n = 5$ and 10 for Fe_{n+1} clusters based on the size dependence of second-order difference of energy, implying that these clusters possess relatively high stabilities. The analysis of atomic net charge Q indicates that the charge always transfers from Fe to Au atom which causes the Au atom to be nearly non-magnetic, and the doped Au atom has little effect on the average magnetic moment of Fe atoms in Fe_nAu cluster. Finally, the total magnetic moment is reduced by 3 μ_B for each of Fe_nAu clusters except $n = 3$, 11, and 12 compared with for corresponding pure Fe_{n+1} clusters.

Keywords: alloy clusters, structures, electronic properties, magnetism

PACS: 31.15.E.–, 36.40.Mr, 36.40.Cg **DOI:** 10.1088/1674-1056/25/6/063103

1. Introduction

Nanoclusters have aroused considerable interest recently, mainly due to their novel electronic and magnetic properties which are different from those of the individual atoms and molecules or bulk matter. Of transition metal clusters, Fe clusters are the most widely studied 3d transition-metal clusters both experimentally[1–5] and theoretically.[6–14] The popularity of iron cluster is attributed to its distinctive reactivity, electronic, magnetic, and catalytic properties[15–21] as cluster size varies. Besides these properties, iron is well known for its high magnetization and an easy conversion to biocompatible oxide, which has received much attention in the biomedical areas.[22–24] At the same time, gold has been regarded as a special research material because of its unique features such as catalytic activity and bio-compatibility.[25–31] Therefore, much attention has been paid to studying the nanostructures comprised of iron and gold in both basic science research and promising application.

The bimetallic Fe/Au nanoparticles have become more popular, which is due mainly to the outstanding physical and chemical properties. Of particular interest is good biocompatibility associated with biological applications. Naturally, based on this reason, a great number of researches have been done. Recently, Liu *et al.*[32] have reported that iron–gold (FeAu) alloy nanoparticles with the optical and magnetic properties present a promising prospect in biological applications. Sun *et al.*[33] studied that the gold-coated iron nanoclusters prevent the iron core from oxidizing, perhaps making a chance to functionalize drug delivery for the magnetic particles. Obviously, Wijaya *et al.*[34] performed magnetic heating experiments of Fe-doped Au nanoparticles and found that the nanoparticles exhibit notable magnetic behavior, presenting a great potential for use in hyperthermia application. Besides, experimental researches about Au–Fe alloys also have been performed in order to explore new nanomaterials in many functional material applications. The optical investigation of AuFe alloys are studied with the Fe concentration range by Gorshunov *et al.*[35] And they observed that the ferromagnetic AuFe clusters give rise to partial localization of conduction electrons. Via a combination of x-ray magnetic circular dichroism (XMCD) experiments and superconducting quantum interference device (SQUID) magnetometries, Wilhelm *et al.*[36] have demonstrated that the Fe in fcc disordered Au–Fe alloy exists in the form of the high-spin state and found the maximum value of magnetic Au moment in bcc Au–Fe alloys. Meanwhile, Crespo *et al.*[37] reported a crucial experiment, showing that Fe impurities weaken the ferromagnetic behavior in Au-contained nanoparticles. Moreover, theoretically, Sternik and Parlinski[38] calculated bilinear coupling constant for Fe_n/Au_m multilayers and observed the increased magnetism of Fe atom, where there is a slight polarization of Au layers. To sum up, the extent to which size, shape, and composition of iron and gold are controlled will be a cruical factor of its flexible applications in magnetic field and biological area.

Based on the above analysis, a considerable number of

*Project supported by the National Natural Science Foundation of China (Grant No. 21301112) and the Ph. D. Program Foundation of the Education Ministry of China (Grant No. 20131404120001).

†Corresponding author. E-mail: lvjin_sxnu@163.com

© 2016 Chinese Physical Society and IOP Publishing Ltd

theoretical researches about Fe–Au alloy clusters have been carried out. Up to now, these investigations mainly focused on the gold-rich Fe–Au alloy clusters aiming at obtaining the desired structural, magnetic, and chemical properties for potential applications. For example, Die *et al.*[39] have investigated single Fe doped gold clusters by using the density-functional theory and summarized the low-energy isomers tending to a two-dimensional structure. Interestingly, Zhang *et al.*[40] revealed doping 3d transition-metal Fe atom into gold cluster that is of planar hexagonal structure where it could stabilize the Au_6 ring and promote the formation of new binary alloy clusters. The stabilities of gold clusters doped with open 3d-shell Fe atom have been investigated by Torres,[41] demonstrating that the electronic and magnetic structure depend on the dopant atom and the geometrical environment. Notably, Yang *et al.*[42] obtained the result that $Fe@Au_{24}$ cluster still keeps the tubular Au_{24} structure with a slight distortion and retains the atom-like magnetism of 4 μ_B, which might be used as new nanomaterials with tunable magnetic properties in the near future. Later, Wang *et al.*[43] found that $Fe@Au_{16}^{-}$ forms a new class of endohedral golden cage cluster which maintains its high spin. In addition, there has been existed apparently on a considerable amount of theoretical work which is focused on the 3d transition metal atoms doped with gold-rich clusters.[39–47] However, to the best of our knowledge, the studies of Au doped with TM-rich along with its dependence of their structures and properties are seriously lacking. It is therefore imperative to obtain a comprehensive understanding of Au doped with TM-rich alloy clusters.

Motivated by the above research background, we carry out the present study on the gold-doped iron clusters Fe_nAu ($n = 1$–12) in order to systematically explore their geometric structures, relative stabilities, electronic and magnetic properties. We attempt to clarify the following points: (i) how the Au doping influences the geometrical structures of the Fe_n cluster, (ii) what the size-dependent growth behavior for Fe_nAu is, (iii) whether some novel properties could be found when one Au atom is doped into iron clusters, (iv) how much is the degree to which the magnetic behavior is changed through incorporating the Au atom and what is the magnetic physics origin responsible for this change. It is expected that in the future, our present work can provide some forceful theoretical guidance in the Stern–Gerlach (SG) experiment, the development of good catalysts for synthesis and the biological and biomedical applications.

2. Computational details

All calculations are performed at the DFT level with the DMol^3 package in the Materials Studio of Accelrys Inc.[48,49] The electron density functional is treated with the generalized gradient approximation (GGA) corrected exchange potential of Perdew, Burke, and Ernzerhof (PBE).[50] The double numerical basis set augmented with d-polarization and p-polarization functions (DNP) is utilized. Relativistic calculations are performed with scalar relativistic corrections to valence orbitals relevant to atomic bonding properties via a local pseudopotential (VPSR).[51] For the numerical integration, a fine quality mesh size is used, and the real space cutoff of the atomic orbital is set to be 5.5 Å. The convergence criteria for structure optimization and energy calculations are set to be fine with the tolerance for electron density and total energy convergence in self-consistent field (SCF), energy, gradient, and displacement of 1×10^{-6} a.u. (The unit a.u. is short for atomic unit), 1.0×10^{-5} a.u., 0.002 a.u., and 0.005 Å, respectively. In the geometry optimization procedure, we consider a number of initial structures including linear chains, planar and three-dimensional structures in this work to maximize our chance to find the ground state configurations of the alloy clusters. First, we identify the low-lying structures of pure Fe_n clusters based on earlier theoretical work on iron[6–14] and other TM clusters,[52–55] and choose these low-lying structures as various reasonable initial structures. Second, on the basis of these initial structures, we substitute the Fe atom with the Au atom at different positions of Fe_{n+1} cluster, and we place the Au atom on each possible site of Fe_n cluster, and also test some structures through referring to Co_nMn/Co_nV,[56,57] Sc_nAl,[58] Fe_nMn,[59] Fe_nCr,[60] Co_nAu,[61,62] Co_nFe,[63] Fe_nPt,[64] and Y_nAl[65] clusters. In this way, we consider more than 400 candidates altogether. Moreover, without any symmetry constrains, we relax the geometric structure to find out the true ground state. Third, for each geometry structure, the magnetic moment is first allowed to optimize automatically into the favored state (S_z) in DMol^3, then, we consider the neighboring spin states ($S_z \pm 2$) or longer-range spin states and optimize them by fixing the spin state. The calculations are implemented until the minimum energy is reached. Finally, subsequent frequency calculations are performed to confirm the optimized geometry corresponding to the minimum value. In addition, for confirming that our obtained low-lying isomers are the most stable isomers in the Fe_nAu clusters, a global search of Fe_7Au cluster based on a particle swarm optimization algorithm within an evolutionary scheme is carried out by using the CALYPSO package.[66] As a result, the most stable structure and metastable state obtained from CALYPSO are consistent with those from our methods mentioned above. The other low-lying isomers are also similar, but only in the order energy there exist some differences. This indicates that the most stable and low-lying isomers our confirmed are indeed in ground state and they are the most stable isomers. Based on the above steps, the net charge and the magnetic moments are evaluated via the Mulliken population analysis.

In order to test the validity of the computational method for the description of Fe_nAu clusters, we first optimize Fe_2 and

Au_2 dimers. All these results are in good agreement with the reported theoretical and experimental results.[1–3,8,13,14,67–71] As listed in Table 1, for Fe_2 the bond length d is 2.02 Å, which is very close to the experimental result of 2.02 ± 0.02 Å[2] (1.87 ± 0.13 Å[1]) and previous theoretical data a of 1.98 Å[13] and 2.008 Å.[8] At the same time, E_b, $\bar{u}$, ω, and IP corresponding to 1.621 eV, 3 μ_B, 418.34 cm^{-1}, and 6.50 eV respectively, are also in good agreement with previous experimental values of 1.64 eV,[13] 3.3 ± 0.5 μ_B,[4] 415 cm^{-1},[8] and 6.30 eV, respectively.[3] Similarly, for Au_2, our calculated $d = 2.49$ Å and $E_b = 1.189$ eV are also in consistent with previous theoretical values (2.49 Å and 1.18 eV[67]). Meanwhile, our caculated ω (181.83 cm^{-1}) and IP (9.41 eV) are similar to the experimental values (191 cm^{-1} and 9.5 eV[69]) and are also in good accordance with previous theoretical calculations (184.2 cm^{-1}, 9.44 eV[67]). All these results indicate that our approach and accuracy are enough to describe the structures and properties of Fe_nAu clusters.

Table 1. Calculated values of bond length d (Å), average binding energy E_b (eV), average magnetic moment $\bar{u}$ (μ_B), vibrational frequency ω (cm^{-1}), and ionization potential IP (eV) of the Fe_2 and Au_2 clusters.

	Fe_2			Au_2		
	Our work	Theoretical	Experimental	Our work	Theoretical	Experimental
d/Å	2.02	1.98[f]	1.87 ± 0.13[a]	2.488	2.49[h]	2.47[i]–[j]
		2.008[e]	2.02 ± 0.02[b]			
E_b/eV	1.621	1.64[f]	0.83∼1.32[k]	1.189	1.18[h]	1.15[i]–[j]
$\bar{u}/\mu_B$	3	3[e]	3.3 ± 0.5[d]	0		
		3[g]				
ω/cm^{-1}	418.34	415[e]	299.6[l]	181.83	184.2[h]	191[i]–[j]
IP/eV	6.50	6.68[e]	6.30[c]	9.41	9.44[h]	9.5[j]
		6.30[g]				

[a] Ref. [1], [b] Ref. [2], [c] Ref. [3], [d] Ref. [4], [e] Ref. [8], [f] Ref. [13], [g] Ref. [14], [h] Ref. [67], [i] Ref. [68], [j] Ref. [69], [k] Ref. [70], [l] Ref. [71].

3. Results and discussion

3.1. Geometrical structures

Using the computational scheme described in Section 2, we have explored a number of low lying isomers and determined the lowest energy structures of Fe_nAu clusters up to $n = 12$. The obtained ground state structures which include these isomers within 0.4 eV of the most stable structure are shown in Fig. 1, together with the symmetries, magnetic moment, and relative energy (ΔE). The point-group symmetry of each cluster is determined using a tolerance of 0.001 Å between the atomic position in the computed structure and the atomic position in the symmetrized reference structure. The lowest energy structures for pure Fe_{n+1} clusters are also considered for comparison. The small Fe_{n+1} clusters up to $n = 12$ are extensively investigated computationally by using DFT. In this work, the geometries for pure iron clusters obtained from the published literatures are reoptimized by using the spin-polarized DFT as described in Section 2. With few exceptions, our calculated structures for $n \leq 6$ agree with published theoretical results,[8–10,13] similar to recently predicted equilibrium structures.[6,9] This reoptimization leads to a slight change in the geometry of the iron clusters. The values of average binding energy (E_b) and the average bond length (d) for the lowest energy structures of Fe_nAu clusters are calculated and listed in Table 2, where the corresponding values for Fe_{n+1} clusters are given in the brackets.

FeAu is $C_{\infty v}$ symmetry dimer, whose bond length and average binding energy are 2.398 Å and 1.552 eV/atom, respectively. These results lie between Fe_2 (2.020 Å, 1.621 eV/atom) and Au_2 (2.488 Å, 1.189 eV/atom). Compared with it of pure Fe_2 (6 μ_B), the magnetic moment of FeAu dimer is reduced by 3 μ_B. Our computed values are in good agreement with the values (2.470 Å and 3 μ_B) obtained in previous paper.[39]

Energetically, the most favorable structure of the Fe_2Au cluster with a total magnetic moment of 7 μ_B is in the form of an isoscele triangle (C_{2v}), whose Fe–Fe distance is 2.073 Å. This may be seen as replacing an Fe atom with an Au atom. Our results about Fe_2Au are proved by Sun *et al.*,[33] whose results show the Fe–Fe distance of 2.020 Å and the same magnetism (7 μ_B). Its metastable state shares the linear chain structure, and the third stable state (9 μ_B) is similar to the ground state. They are energetically less stable by 0.020 eV and 0.124 eV, respectively.

A planar structure (C_{2v}) is the most stable Fe_3Au cluster with 9 μ_B of total magnetic moment. The second energetically degenerate structure (9 μ_B), which is of a turnup rhombus (four atoms are not on the same plane) structure (C_s), is energetically less favorable than the most stable structure in energy by 0.062 eV. The third lowest-energy structure is similar to the most stable structure, but they differ by 11 μ_B of total magnetic moment. A distorted tetrahedronal configuration with C_s symmetry is the fourth stable isomer. The energy is 0.382 eV less stable in energy compared the lowest energy structure, which means that there is the turning from the planar (2D) structure to the three-dimensional (3D) structure.

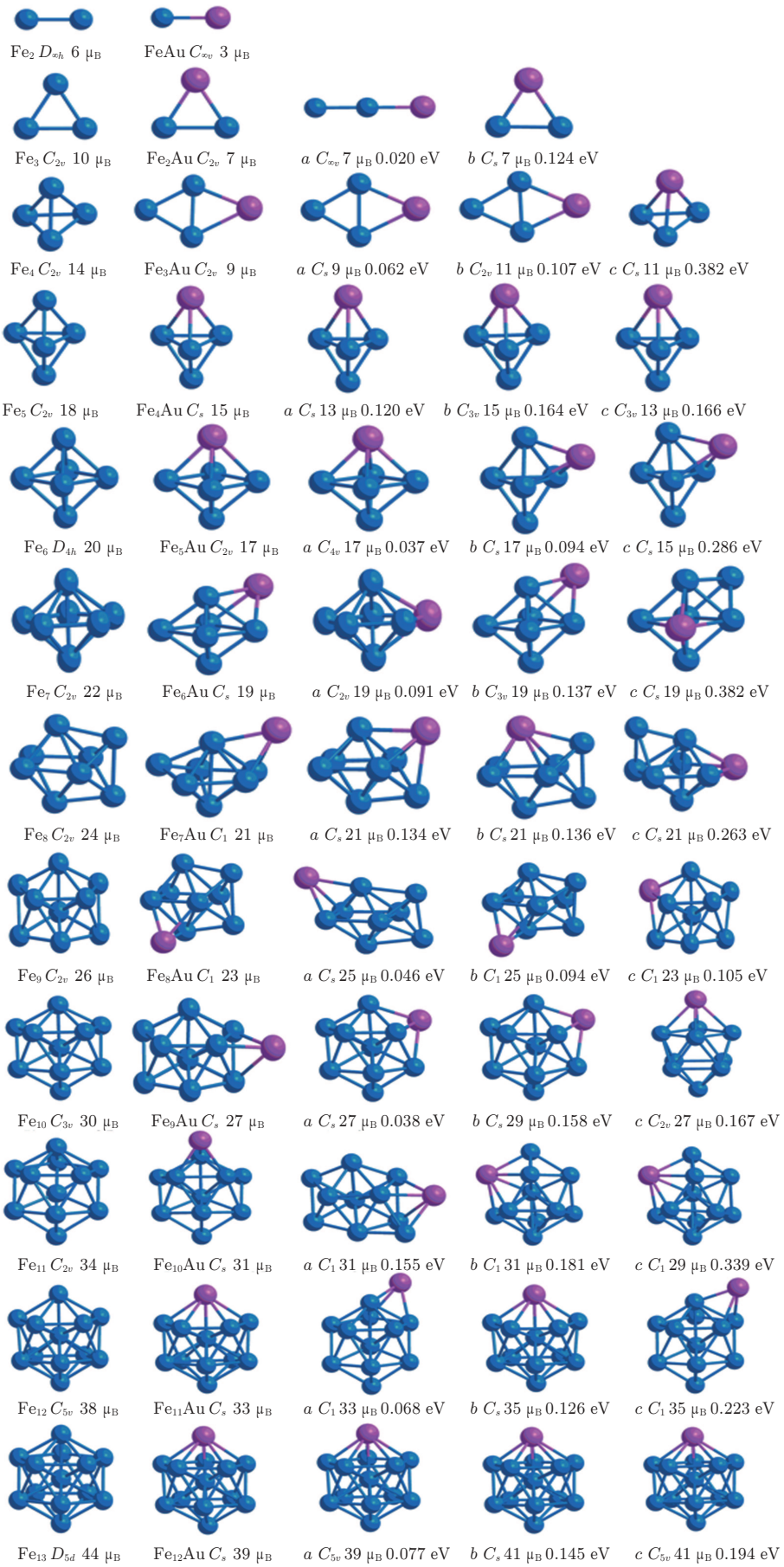


Fig. 1. (color online) Lowest-energy structures and low-lying isomers with different relative energies (in unit eV) of Fe$_n$Au (n = 1–12) clusters. The ground state geometries of the corresponding bare Fe$_{n+1}$ clusters are also given on the left. The blue and pink balls represent Fe and Au, respectively. Distances are given in unit Å.

Table 2. Values of average binding energy (E_b), average bond length (d), average magnetic moment at Fe atom ($\bar{u}_{atom}$), HOMO–LUMO (highest occupied molecular orbital–lowest unoccupied molecular orbital) gaps in the lowest energy structures of Fe_nAu clusters. Corresponding values for Fe_{n+1} cluster are given in the brackets.

Cluster	E_b/(eV/atom)		d/Å		$\bar{u}_{atom}$		Gap/eV
FeAu	1.552	(1.621)	2.398	(2.020)	3.040	(3.000)	0.040
Fe_2Au	2.001	(2.089)	2.394	(2.271)	3.301	(3.333)	0.485
Fe_3Au	2.433	(2.516)	2.366	(2.353)	3.010	(3.500)	0.506
Fe_4Au	2.736	(2.848)	2.450	(2.398)	3.667	(3.600)	0.404
Fe_5Au	2.970	(3.103)	2.450	(2.400)	3.341	(3.333)	0.376
Fe_6Au	3.144	(3.252)	2.448	(2.391)	3.163	(3.143)	0.475
Fe_7Au	3.251	(3.337)	2.446	(2.426)	3.000	(3.000)	0.452
Fe_8Au	3.318	(3.387)	2.429	(2.393)	2.885	(2.889)	0.423
Fe_9Au	3.395	(3.445)	2.455	(2.434)	2.980	(3.000)	0.393
$Fe_{10}Au$	3.453	(3.516)	2.477	(2.454)	3.086	(3.091)	0.120
$Fe_{11}Au$	3.521	(3.576)	2.484	(2.476)	2.983	(3.167)	0.204
$Fe_{12}Au$	3.586	(3.657)	2.514	(2.504)	3.076	(3.385)	0.126

In the case of Fe_5, we find the C_{2v} triangular bipyramid structure to have the lowest energy. For Fe_4Au, the overall structures are totally retained, but they are slightly distorted triangular bipyramid with the Au atom at the vertex. The most stable isomer is of C_s symmetry and it has a total magnetic moment of 15 μ_B, which is reduced by 3 μ_B in comparison with the pure Fe_5 (18 μ_B). By contrast, the second stable structure (C_s) with a total magnetic moment of 13 μ_B is 0.120 eV evidently higher in energy. The other two stable isomers (C_{3v}) have total magnetic moments of 15 μ_B and 13 μ_B, and 0.164 eV and 0.166 eV above the lowest-energy structure, respectively.

The C_{2v} configuration of Fe_5Au with the magnetism (17 μ_B) is found to be the most stable isomer, which may be viewed as a deviation from substitution of a Fe atom by an Au atom in the octahedron Fe_6 (D_{4h}) structure. The other distorted octahedron geometrical isomer with C_{4v} symmetry is considered to be the second stable structure at a slightly higher energy (0.037 eV). Differently, the following two stable isomers prefer to share a capped triangle bipyramid with Au atom being at the cap position, which are located at 0.094 eV and 0.286 eV in energy above the most stable conformation.

For the Fe_6Au clusters, we consider a lot of initial geometries including the bicapped triangular bipyramid, capped octahedron, pentagonal bipyamid, bicapped square pyramid, etc. At last, an Au-capped octahedron structure with C_s symmetry is found to have the lowest energy. However, the metastable state is a distorted pentagonal bipyramid (C_{2v}) with the impurity Au atom in the middle pentagonal ring plane, and is found to be only 0.091 eV less stable than the ground state. The third state also favors a capped octahedron (C_{3v}) and is energetically less favorable than the most stable structure by 0.137 eV. The fourth state is still a capped octahedron (C_s) with the Au atom at the square site, and is 0.382 eV higher in total energy. Moreover, we notice that these four stable structures of Fe_6Au have the equal total magnetic moment (19 μ_B).

Energetically the most favorable structure for Fe_7Au (21 μ_B) is an Au-capped distorted pentagonal bipyramid with C_1 symmetry. The metastable state with a classic bicapped octahedron structure is 0.134 eV in energy higher than the lowest-energy structure. As seen in Fig. 1, the third lowest-energy structure is still a bicapped octahedron with an Au atom at the vertex position of the octahedron. It has the same magnetism as the ground state structure and is 0.136 eV higher in energy. A capped-pentagon bipyramid (21 μ_B), where Au atom becomes a part of the pentagonal ring, is regarded as the fourth stable isomer and has a high relative energy of $\Delta E = 0.263$ eV.

In the case of $n = 8$, the most stable Fe_8Au (23 μ_B) with C_1 symmetry is capped one Au atom on the Fe_8 ground-state geometry. The second stable isomer and the third stable isomer have similar geometric configurations with the lowest-energy structure but Au atoms occupy the different capped positions, whose total energies are only 0.046 eV and 0.094 eV above the lowest-energy isomer. The last stable isomer (C_1) with a total magnetic moment of 23 μ_B can be viewed as the Fe atom in the ground state structure of Fe_9 replaced by one Au atom.

For the case of Fe_9Au, the lowest-energy structure with C_s symmetry prefers one capping Au atom on the surface of the ground-state Fe_9 cluster. As shown in Fig. 1, Au atom substituting one Fe atom of a three-capped pentagonal bipyramid structure of Fe_{10} cluster yields the second and third stable structure of the Fe_9Au cluster with the C_s symmetry, and are 0.038 eV and 0.158 eV in energy less favorable than the most stable structure, respectively. The last stable structure with C_{2v} symmetry is formed by capping one Au atom on tri-capped triangular prism, which is 0.167 eV higher in energy than the ground state.

In terms of $Fe_{10}Au$ (C_s), the most stable structure is similar to that of the Fe_{11} cluster which is a tetra-capped pentagonal bipyramid with the Au atom at the vertex position. It has

a total magnetic moment 31 μ_B, and is 0.155 eV in energy lower than that of the metastable state. As seen in Fig. 1, the third and the fourth lowest energy structure which can be regarded as Au replacing one Fe atom of the Fe_{11} cluster have the same geometry but different magnetisms, and are 0.181 eV and 0.339 eV above the lowest-energy structure, respectively.

Just like the Fe_{12} cluster, the lowest-energy structure of $Fe_{11}Au$ cluster takes an icosahedral growth pattern where Au atom substitutes the Fe site at the apex with a total magnetic moment of 33 μ_B as shown in Fig. 1. Differently, an Au atom capping a peripheral position of the Fe_{11} cluster produces the second and the fourth lowest-energy structure, where relative energies are 0.068 eV and 0.223 eV, respectively. In comparison, the third lowest-energy structure takes a similar geometry to the most stable structure but the increased magnetic moment (35 μ_B) and is located at 0.114 eV in energy above the ground state.

With regard to $Fe_{12}Au$ cluster, we consider the icosahedral, hexagonal close packed (hcp), rhombic dodecahedral (bcc) and cuboctahedral (fcc) structures as initial geometries. Overall, the most stable configurations we have finally obtained can be looked upon as a substitutional Au impurity in the pure Fe_{13} cluster, in which Au atom lies at the one vertex site of the icosahedral structure. As shown in Fig. 1, the other low-lying isomers (*a*, *b*, *c*) have notable instablities (0.077, 0.145, and 0.194 eV, respectively).

The overall evolutionary trends for the Fe_nAu series show that for $n = 1$–2, 4–5, 10–12, the Au doped geometries are similar to those of Fe_{n+1} clusters, where the Au atom occupies a substitutional surface site accompanied with a slight distortion in the host cluster. And the way of growing Fe_nAu ($n = 6$–9) clusters is that the Au atom occupies a peripheral position of Fe_n cluster. This phenomenon can be attributed to the two aspects: on the one hand, Au atom prefers to occupy peripheral location, which can be explained by the cohesive energy (CE) and the surface energy (SE) of the metal atom. To minimize the total energy, the atom with the smaller surface energy and cohesive energy tends to occupy the surface, while the atom with a higher surface energy and cohesive energy favors the interior[72–74] The surface energy and average cohesive energy of the bulk Au are 1.506 J·m^{-2} and 3.81 eV/atom, which are smaller than those of the bulk Fe 2.417 J·m^{-2} and 4.28 eV/atom respectively.[75,76] On the other hand, the atomic size effect also accounts for this. The smaller atoms tend to occupy the more sterically confined core, especially in icosahedral clusters, exhibiting the compression effects finally forming a stable cluster.[72] The atomic radius of Au is larger than that of Fe atom.[75] Thus, the Fe atoms prefer to occupy central position, whereas the Au atom prefers to be located at the site of surface. Similar phenomena and explanations also appeared in previous studies.[61,76–79]

3.2. Relative stabilities

In this subsection, we will investigate the size-dependent physical properties of these clusters. The variation of average binding energy $E_b(n)$ with cluster size is shown in Fig. 2(a). For comparison, we also show the variation of $E_b(n)$ with cluster size for pure iron cluster. The average binding energy $E_b(n)$ is defined as

$$E_b(Fe_nAu) = [nE(Fe) + E(Au) - E(Fe_nAu)]/(n+1), \quad (1)$$

$$E_b(Fe_{n+1}) = [(n+1)E(Fe) - E(Fe_{n+1})]/(n+1), \quad (2)$$

where E is the total energy of the respective atoms or clusters. From Fig. 2(a), it can be seen that the E_b rises monotonically with increasing the sizes of both Fe_{n+1} and Fe_nAu clusters. This is because both the average coordination number and the effective hybridization increase as cluster size n increases. Especially, the average binding energy of Fe_{n+1} clusters increases towards the cohesive energy of bulk Fe solid (4.280 eV/atom) with cluster size growing. Meanwhile, in the beginning stage for $n = 1$–6, E_b of Fe_nAu clusters increases rapidly; when n goes from 7 to 12, the E_b increases with size n increasing, but finally tend to saturation and convergence. Despite all this, the E_b of the Fe_nAu cluster is 0.050 eV–0.133 eV smaller than that of Fe_{n+1}, indicating the decrease of the

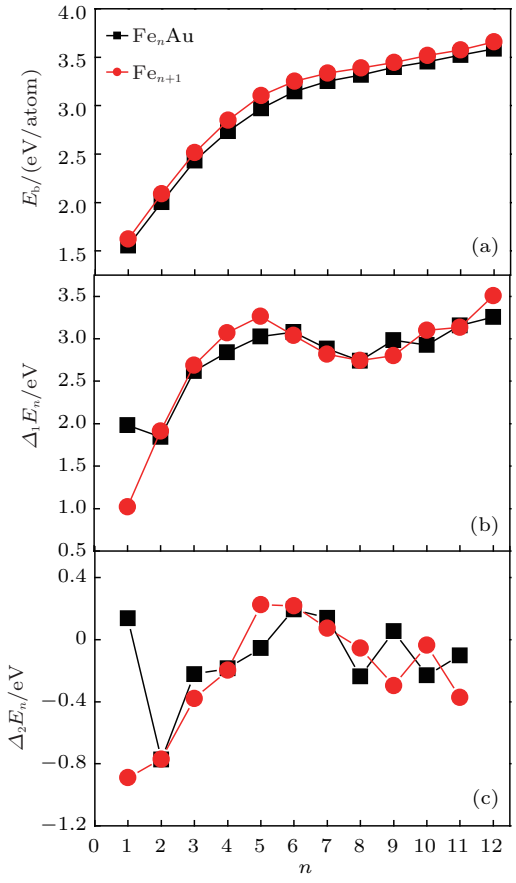


Fig. 2. (color online) Size dependences of averaged atomic binding energies (a), fragmentation energies (b), and second-order difference energies (c) for the lowest energy structures of Fe_nAu and Fe_{n+1} ($n = 1$–12) clusters.

stability of iron clusters after Au doping. We infer that a reduction of E_b could be attributed to the following two reasons: (i) the cohesive energy of bulk Fe (4.28 eV) is significantly larger than bulk Au (3.81 eV), indicating that the stability of pure Fe_{n+1} cluster is weakened after one Au atom doping. Based on the above analysis, the trend of E_b of our calculated dimers is Fe_2 (1.621 eV) > FeAu (1.552 eV) > Au_2 (1.189 eV), which is consistent with the cohesive energy of bulk; (ii) much longer average bond lengths of doping clusters, which generates a weaker Fe–Au bond than the Fe-Fe bond (as seen in Table 1).

In cluster physics, the fragmentation energies and second-order difference of energies are sensitive indicators of the relative stability. Thus, the size dependence of the fragmentation energies and second-order difference of energies for Fe_nAu ($n = 1$–12) clusters are further investigated. The fragmentation energy $\Delta_1 E(n)$ and the second-order difference energy $\Delta_2 E(n)$ are calculated using the following formulas:

$$\Delta_1 E(\mathrm{Fe}_{n+1}) = E(\mathrm{Fe}_n) + E(\mathrm{Fe}) - E(\mathrm{Fe}_{n+1}), \quad (3)$$

$$\Delta_2 E(\mathrm{Fe}_{n+1}) = E(\mathrm{Fe}_{n+2}) + E(\mathrm{Fe}_n) - 2E(\mathrm{Fe}_{n+1}), \quad (4)$$

$$\Delta_1 E(\mathrm{Fe}_n\mathrm{Au}) = E(\mathrm{Fe}_{n-1}\mathrm{Au}) + E(\mathrm{Fe}) - E(\mathrm{Fe}_n\mathrm{Au}), \quad (5)$$

$$\Delta_2 E(\mathrm{Fe}_n\mathrm{Au}) = E(\mathrm{Fe}_{n+1}\mathrm{Au}) + E(\mathrm{Fe}_{n-1}\mathrm{Au}) - 2E(\mathrm{Fe}_n\mathrm{Au}), \quad (6)$$

where $E(\cdot)$ is the respective atoms or clusters. Based on the above formulas, the evolutions of $\Delta_1 E(n)$ and $\Delta_2 E(n)$ are plotted in Figs. 2(b) and 2(c). Obviously, the local peaks of the fragmentation energies and second-order difference of energies are localized at $n = 6$ and 9, indicating that Fe_6Au and Fe_9Au clusters are more stable than the other isomers. The high stability of Fe_6Au may mainly stem from the Au capping a similar compact octahedral Fe_6 core. Meanwhile, it is clearly seen that both curve of the fragmentation energies and curve of the second-order difference of energies reach their maxima at $n = 5$ and 10, indicating that the clusters of Fe_6 and Fe_{11} are the most stable structures among our investigated Fe_{n+1} ($n = 1$–12) clusters. The magic stability of Fe_6 cluster has appeared in previous studies.[8,10]

In addition, the HOMO–LUMO gap is a characteristic quantity of electronic structure in clusters and is commonly used to measure the ability for clusters to undergo activated chemical reactions with small molecules. A big energy gap usually corresponds to a high chemical stability. As shown in Fig. 3, FeAu cluster has the narrowest HOMO–LUMO gap, which is only 0.040 eV. However, the gap change trend for Fe_nAu ($n = 2$–9) clusters which are bigger in energy gap (0.376 eV–0.506 eV) almost keeps a relatively stable value, indicating their high chemical inertness. There are three dramatic drops at $n = 10$, 11, and 12. The decreases of the gaps (0.120 eV–0.204 eV) suggest that more atoms are involved in the metal-metal bonding.[80,81] Thus, these clusters could have potential utility in new cluster catalysis nanomaterials as building block with reactive and metallic properties.

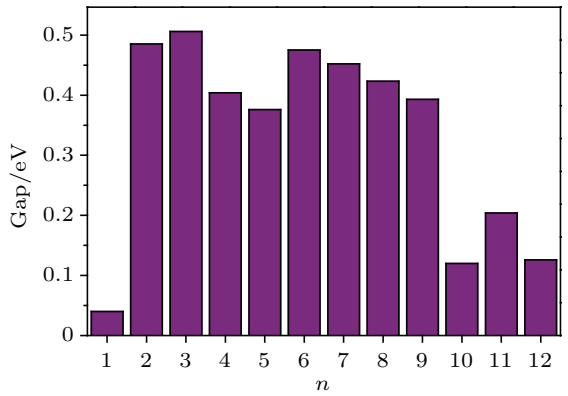


Fig. 3. (color online) HOMO–LUMO gaps of the most stable structures of Fe_nAu clusters as function of cluster size.

The magnetic stability of these clusters can be verified by calculating the spin gaps as a function of the cluster size. The spin gaps for a magnetic cluster are defined as

$$\delta_1 = -(\varepsilon_{\mathrm{HOMO}}^{\mathrm{majority}} - \varepsilon_{\mathrm{LUMO}}^{\mathrm{minority}}), \quad (7)$$

$$\delta_2 = -(\varepsilon_{\mathrm{HOMO}}^{\mathrm{minority}} - \varepsilon_{\mathrm{LUMO}}^{\mathrm{majority}}), \quad (8)$$

where $\varepsilon_{\mathrm{HOMO}}^{\mathrm{majority}}$ and $\varepsilon_{\mathrm{LUMO}}^{\mathrm{majority}}$ are the HOMO level and LUMO level of the majority spin density, $\varepsilon_{\mathrm{HOMO}}^{\mathrm{minority}}$ and $\varepsilon_{\mathrm{LUMO}}^{\mathrm{minority}}$ are the HOMO level and LUMO level of the minority spin density, respectively. The magnitude of spin gap is a measure of the chemical activeness of cluster: the higher the spin gap, the more stable the cluster is. As seen from Fig. 4, both δ_1 and δ_2 of Fe_nAu ($n = 1$–12) clusters are positive, indicating that those clusters are magnetically stable. Moreover, the δ_1 and δ_2 values are found to decrease as size increases. The higher spin gaps of the small size clusters are attributed to the quantum size effect.[82]

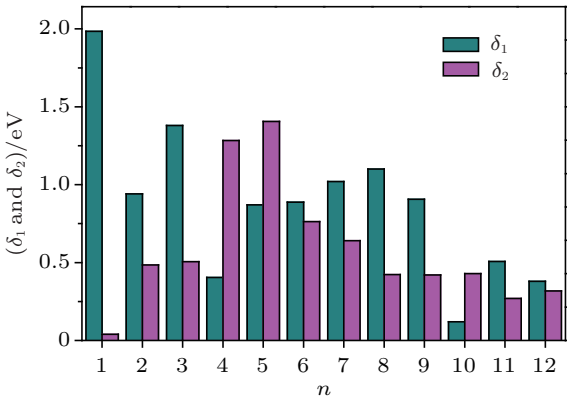


Fig. 4. (color online) Size dependences of the spin gaps of Fe_nAu ($n = 1$–12) clusters.

3.3. Magnetic moments

The total magnetic moments of the ground-state Fe_nAu ($n = 1$–12) clusters are calculated and the results are presented in Fig. 5(a). These results show that the total magnetic moments of the ground-state Fe_nAu ($n = 1$–12) clusters are 3 μ_B

smaller than those of the pure Fe_{n+1} with three exceptional jumps of 5 μ_B (Fe_3Au, $Fe_{11}Au$, and $Fe_{12}Au$). The valence electron configurations of the free atoms Fe and Au are $3d^64s^2$ and $4f^{14}5d^{10}6s^1$, respectively. For an isolated Fe (Au) atom, the magnetic moment is 4 μ_B (1 μ_B) based on the Hund's rule. Taking the ferromagnetic alignment into account on the Fe_{n+1} and most of Fe_nAu clusters, the unpaired electrons of Fe_{n+1} and Fe_nAu clusters will be $4(n+1)$ and $4n+1$, respectively. Therefore, the magnetic moments of the Fe_nAu clusters are supposed to decrease by 3 μ_B. A similar explanation can be found in the studies of $Co_{n-1}Mn$ and $Co_{n-1}V$ clusters.[56] In addition, the average magnetic moments of Fe atom for ground state Fe_{n+1} and Fe_nAu clusters are also plotted in Fig. 5(b). It can be seen that the Fe atomic average magnetic moment remains almost unchanged for the case of Au doping, which still keeps about 3 μ_B of magnetism of pure Fe_{n+1} clusters. However, the magnetism of Fe_nAu clusters is reduced by 5 μ_B compared with that of the corresponding pure Fe_{n+1} clusters, and Fe atomic average magnetic moment of Fe_nAu clusters decreases largely.

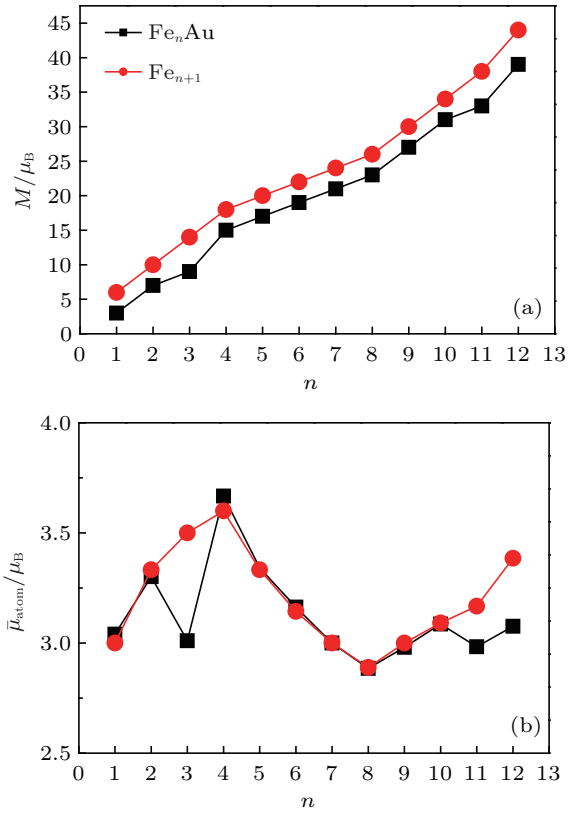


Fig. 5. (color online) Size dependences of the magnetic moments (a) and the average magnetic moments of Fe atom (b) for Fe_nAu and Fe_{n+1} ($n = 1$–12) clusters.

As shown in Fig. 6, the average bond lengths and average coordination numbers display a similar trend as a function of the cluster size, which is due to their similar geometrical structures. Evidently, in the initial stage for $n = 1$–4, their average bond lengths increase rapidly, when n goes from 4 to 8, become relatively stable, as n goes from 8 to 12, they increase gradually again. And yet, the average coordination numbers always increase gradually. As is well known, the larger the bond length, the larger the magnetic moment of cluster is, on the contrary, the larger the coordination numbers, the smaller the magnetic moment of cluster is. The consequence of mutual competition of the two factors ultimately determines the most stable structure of each cluster size.[83,84] Thus, as shown in Fig. 5(b), the average magnetic moment of the Fe_n and Fe_nAu presents an increasing trend in $n = 1$–4 decreases rapidly in $n = 4$–8 increases gradually again in $n = 8$–12. This indicates that the average bond length is dominant in influencing the magnetism of the clusters.

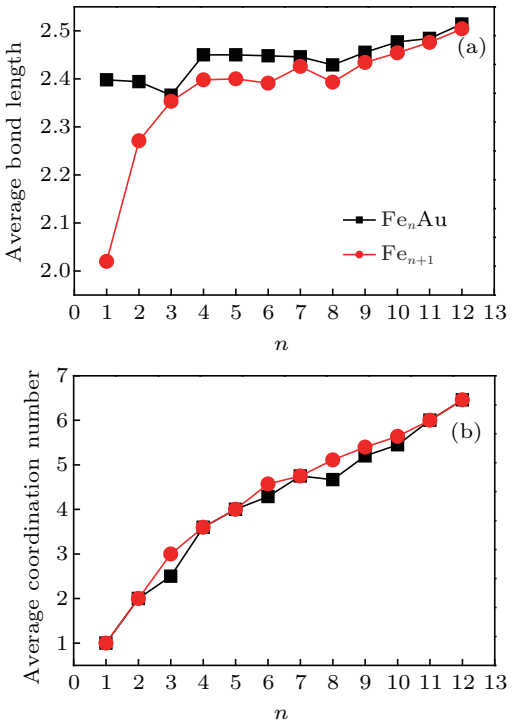


Fig. 6. (color online) Variations of average bond length (a) and average coordination number (b) with the cluster size for Fe_nAu and Fe_{n+1} ($n = 1$–12) clusters.

The reason why the Fe atomic average magnetic moments of $n = 3$, 11, and 12 alloy clusters obviously decrease compared with that of pure Fe clusters is explained in detail. It can be seen from Fig. 6 that for $Fe_{12}Au$ and Fe_{13}, the average bond lengths remain almost unchanged and average coordination numbers are the same. So the reason most likely is the result of the symmetry. Researches about clusters pointed out that the higher the symmetry, the bigger the magnetic moment is.[85,86] Generally, the higher symmetry of a cluster forms a narrow d electronic state, which leads to spin splitting more easily, and become a more parallel d electronic spin, consequently generating larger magnetism. Since one Fe atom is substituted by one Au atom at the apex of the icosahedron, the symmetry C_s of $Fe_{12}Au$ is lower than D_{5d} of Fe_{13}. Thus, the average magnetic moment of Fe atom obviously decreases with respect to pure Fe cluster. This explanation is suitable for $Fe_{11}Au$ clus-

ter. However, Fe_3Au does not have the close-packed tetrahedron geometric structure, but has the complete plane rhombic geometric construction where the dihedral angle is 0 degree. Therefore, Fe_4 with its relative close-packed tetrahedron geometric structure exhibits the stronger spin polarization, while the spin polarization of Fe_3Au is sharply weakened, finally leading to the fact that the average magnetic moment of Fe atom of Fe_3Au cluster is attenuated compared with that of the pure Fe_4 cluster.

For the optimized geometry structure, the total magnetic moments of Fe_nAu clusters, the local moments of Fe and Au atoms, the atomic net charges and the local moments of 3d, 4s, and 4p states for Fe and Au atoms are calculated and summarized in Table 3. The local magnetic moment of per Fe

Table 3. Atom labels and values of atomic net charge Q (e), local magnetic moment $\mu_{\rm atom}$ ($\mu_{\rm B}$) of the atom, Mulliken charge (e), and local magnetic moment of s, p, and d states μ_L ($\mu_{\rm B}$) for the lowest energy structures of Fe_nAu ($n = 1$–12) clusters.

Clusters	Atom label	Q	$\mu_{\rm atom}$	Mulliken charge/$\mu_{\rm L}$			$M/\mu_{\rm B}$
				3d/5d	4s/6s	4p/6p	
$1/C_{\infty v}$	Au(1)	-0.258	–0.04	9.812/0.062	1.411/–0.117	0.039 / 0.016	3
	Fe(2)	0.258	3.04	6.837/3.099	0.838/–0.064	0.067/0.005	
$2/C_{2v}$	Au(1)	–0.322	0.399	9.678 /0.120	1.496/0.220	0.153 /0.059	7
	Fe(2,3)	0.161	3.300	6.757/3.100	0.834/0.148	0.244/0.057	
$3/C_{2v}$	Fe(1,3)	0.162	2.973	6.815/2.989	0.698/–0.008	0.319/–0.002	
	Fe(2)	–0.001	3.084	6.761/3.035	1.067/0.076	0.170/–0.022	9
	Au(4)	–0.323	–0.030	9.716/0.035	1.468/ –0.047	0.144/–0.018	
$4/C_s$	Fe(1,5)	0.065	3.769	6.576/3.282	0.821/0.262	0.534/0.232	
	Au(2)	–0.220	0.333	9.620 /0.158	1.315/0.048	0.291/0.127	15
	Fe(3)	0.044	3.653	6.636/3.193	0.782/0.249	0.533/0.218	
	Fe(4)	0.045	3.476	6.699/3.171	0.831/0.104	0.422/0.207	
$5/C_{2v}$	Fe(1)	–0.020	3.191	6.776/3.010	0.735/0.089	0.505/0.099	
	Fe(2,3)	0.057	3.361	6.672/3.158	0.821/0.101	0.446/0.108	17
	Au(4)	–0.224	0.295	9.579/0.155	1.265/0.088	0.387/0.053	
	Fe(5,6)	0.065	3.396	6.693/3.121	0.725/0.161	0.512/0.121	
$6/C_s$	Fe(1,2)	0.013	3.208	6.743/3.060	0.826/0.069	0.415/0.086	
	Fe(3)	0.033	2.972	6.805/2.859	0.594/0.049	0.562/0.071	
	Fe(4)	–0.048	3.116	6.777/2.955	0.721/0.085	0.562/0.071	19
	Fe(5,6)	0.127	3.237	6.711/3.074	0.697/0.071	0.546/0.083	
	Au(7)	–0.264	0.022	9.677/0.070	1.341/–0.059	0.253/0.011	
$7/C_1$	Fe(1)	–0.019	3.069	6.788/2.972	0.825/0.050	0.401/0.055	
	Fe(2)	–0.047	2.888	6.826/2.847	0.836/0.027	0.381/0.020	
	Fe(3)	–0.019	3.071	6.787/2.974	0.826/0.049	0.402/0.055	
	Fe(4)	0.077	3.074	6.784/2.961	0.706/0.046	0.427/0.074	21
	Fe(5)	0.078	3.069	6.785/2.958	0.705/0.045	0.426/0.074	
	Fe(6)	0.175	2.887	6.787/2.826	0.583/0.010	0.449/0.048	
	Fe(7)	0.040	2.953	6.777/2.891	0.646/0.033	0.532/0.036	
	Au(8)	–0.283	–0.001	9.684/0.054	1.377/–0.055	0.229/0.001	
$8/C_1$	Fe(1)	–0.069	2.802	6.863/2.785	0.835/0.013	0.367/0.010	
	Fe(2)	–0.036	3.004	6.807/2.948	0.834/0.020	0.391/0.043	
	Fe(3)	0.146	2.904	6.805/2.843	0.600/0.029	0.445/0.040	
	Fe(4)	0.033	2.875	6.849/2.824	0.684/0.014	0.429/0.044	
	Fe(5)	0.034	3.005	6.783/2.927	0.734/0.053	0.446/0.032	23
	Fe(6)	0.183	2.713	6.837/2.686	0.578/0.008	0.398/0.026	
	Fe (7)	0.061	2.845	6.823/2.816	0.630/0.013	0.482/0.024	
	Au(8)	–0.286	–0.077	9.682/0.046	1.370/–0.117	0.241/–0.006	
	Fe(9)	–0.065	2.928	6.859/2.834	0.802/0.041	0.400/0.060	
$9/C_s$	Fe(1,3)	0.031	3.003	6.791/2.957	0.730/0.018	0.443/0.035	
	Au(2)	–0.320	0.179	9.655/0.081	1.457/0.061	0.214/0.038	
	Fe(4,6)	–0.014	3.088	6.795/2.961	0.781/0.060	0.434/0.075	
	Fe(5)	0.014	2.949	6.778/2.886	0.681/0.024	0.523/0.047	27
	Fe(7)	0.225	2.698	6.778/2.685	0.629/–0.022	0.363/0.041	
	Fe(8)	0.169	2.902	6.800/2.841	0.612/0.011	0.415/0.056	
	Fe(9,10)	–0.061	3.044	6.794/2.946	0.866/0.037	0.415/0.056	
$10/C_s$	Au(1)	–0.346	0.142	9.652/0.095	1.473/–0.006	0.227/0.054	
	Fe(2,9)	–0.076	3.233	6.747/3.052	0.937/0.103	0.389/0.084	
	Fe(3,10)	–0.068	3.191	6.748/2.979	0.845/0.10	0.471/0.113	
	Fe(4)	0.001	3.072	6.797/2.913	0.703/0.036	0.494/0.131	31
	Fe(5,6)	0.164	2.930	6.810/2.868	0.640/0.006	0.382/0.063	
	Fe(7)	0.311	2.731	6.803/2.768	0.600/–0.068	0.280/0.037	
	Fe(8)	0.073	3.026	6.783/2.915	0.647/0.018	0.491/0.100	
	Fe(11)	–0.078	3.322	6.725/3.036	0.920/0.148	0.429/0.144	

Table 3. (*continued*)

Clusters	Atom label	Q	μ_{atom}	Mulliken charge/μ_L			M/μ_B
				3d/5d	4s/6s	4p/6p	
11/C_s	Fe(1,3)	0.009	3.031	6.790/2.897	0.737/0.050	0.457/0.092	
	Fe(2,4)	–0.083	3.142	6.757/2.998	0.854/0.065	0.469/0.087	
	Fe(5)	–0.007	3.021	6.820/2.917	0.754/0.040	0.428/0.071	
	Fe(6)	–0.040	3.126	6.759/2.914	0.773/0.085	0.504/0.135	
	Fe(7,9)	–0.053	3.093	6.763/2.967	0.836/0.040	0.450/0.092	33
	Fe(8,10)	–0.021	3.016	6.790/2.882	0.730/0.033	0.495/0.110	
	Fe(11)	0.681	2.107	6.981/2.263	0.579/–0.098	–0.249/–0.052	
	Au(12)	–0.338	0.182	9.596/0.076	1.326/0.073	0.425/0.032	
12/C_s	Fe(1,11)	–0.055	3.221	6.745/2.994	0.771/0.069	0.535/0.166	
	Fe(2)	–0.067	3.342	6.703/3.037	0.817/0.123	0.542/0.190	
	Fe(3,7)	–0.053	3.395	6.681/3.090	0.829/0.142	0.540/0.171	
	Fe(4,6)	–0.032	3.393	6.692/3.085	0.813/0.157	0.523/0.159	
	Fe(5)	–0.013	3.466	6.660/3.116	0.801/0.161	0.549/0.197	
	Fe(8)	–0.041	3.464	6.651/3.113	0.817/0.148	0.570/0.211	39
	Fe(9,12)	–0.026	3.190	6.754/2.981	0.759/0.066	0.508/0.150	
	Au(10)	–0.331	0.237	9.553/0.096	1.271/0.073	0.519/0.068	
	Fe(13)	0.783	2.093	7.073/2.388	0.640/–0.122	–0.509/–0.168	

(Au) is the summation of the differences in number between spin-up and spin-down 3d/4s/4p (5d/6s/6p) electrons. The spin magnetic moment of an electron is 1 μ_B.[83] The atom label is presented in Fig. 7. It can be seen from Table 3 that all of the atoms in the ground states of Fe$_n$Au alloy clusters are aligned ferromagnetically except for FeAu, Fe$_3$Au, and Fe$_8$Au. At the same time, the magnetic moments of the alloy clusters are mainly manipulated by the 3d electrons whereas the s and p electrons contribute only a small amount of net spin. For Fe$_n$Au clusters, the 4s state of Fe and 5d state of Au all lose some electrons, meanwhile 3d, 4p states of Fe and 6s, 6p states of Au gain extra electrons (see in Table 3). It therefore means that there happens s-pd hybridization in the Fe and Au atoms. As a result, the local magnetic moments of Fe and Au in Fe$_n$Au clusters are attenuated compared with those of their free atoms. From the analysis of atomic net charge Q, we find that the charge always transfers from Fe to Au atom, which is consistent with the empirical Pauling electronegativities (χ_p(Fe) = 1.83 eV, χ_p(Au) = 2.54 eV). Thus, this trend of charge transfer leads to the Au atom being nearly nonmagnetic. The above results imply that the charge transfer and the strong hybridization between Fe 4s, 3d and Au 6s, 6p, 5d states might be one major reason for inducing magnetism of Fe$_n$Au cluster.

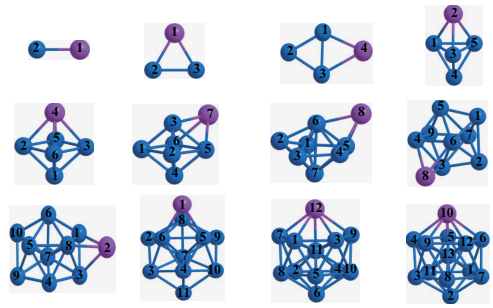


Fig. 7. (color online) Atom labels of the ground state of Fe$_n$Au (n = 1–12) clusters.

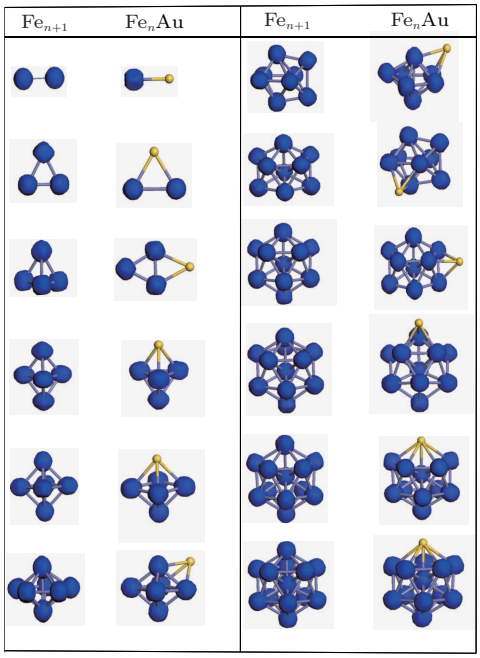


Fig. 8. (color online) spin densities of Fe$_n$Au and Fe$_{n+1}$ (n = 1–12) clusters. The density isosurfaces are drawn at 0.5 a.u.

To gain an insight into the magnetism of the Fe$_n$Au cluster, we also explore the spin densities of the alloy clusters. In Fig. 8, for proper comparison, we plot the differences between the charge density for spin-up electrons and that of spin-down electrons for Fe$_{n+1}$ (n = 1–12) clusters. As seen from Fig. 8, the contributions to magnetism of the cluster mainly originate from Fe atoms in Fe$_n$Au and the Au atom has no influence on magnetism. Meanwhile, the spin density volume of the Fe atom has almost no change after substituting an Fe atom with an Au atom, which means that the local magnetic moment of Fe in Fe$_n$Au is nearly equal to those in Fe$_{n+1}$ (n = 1–12) clusters. Meanwhile, the doping-Au atom has no spin density, which is consistent with the fact that the Au atom is almost

nonmagnetic. In addition, to further ascertain the reason for reducing the magnetic moment, we perform detailed analyses of spin polarization (P) of Fe atomic d orbital for Fe_{n+1} and Fe_nAu alloy clusters in the Supporting Information Table S1. The results show that the average spin polarizations of d orbital of Fe atom for Fe_{n+1} and Fe_nAu alloy clusters are almost identical. Therefore, doping with the Au atom results in reducing the total magnetic moment of Fe_nAu clusters, while it has no effect on the local magnetic moment of Fe atom.

In order to explore the magnetic origin further, In Fig. 9, we present the s-, p-, and d-projected partial densities of states (PDOSs) and local densities of states (LDOSs) of Fe_{11} and $Fe_{10}Au$ clusters as representatives. (See the Supporting Information about the PDOS and LDOS contributions of Fe_{13} and $Fe_{12}Au$ clusters). It is clearly seen that the magnetic moments of these clusters mainly come from d states, while the s and p states only contribute a small amount of net spin, which is in good agreement with the above Mulliken population analyses of the on-site atomic charges and the atomic spin density. For Fe_{11}, we find that the up- and down-spin channels of the d PDOS are seriously asymmetric, which has a magnetic moment of 34 μ_B. Substituting Fe atom by Au reduces the up-spin channel, and a small peak of the down-spin d PDOS is broadened around −4.2 eV below the Fermi level, which consequently enhances significantly the depletion of down-spin d states, finally leading to the total magnetic moment reducing 3 μ_B. In addition, the up-spin channels of $Fe_{10}Au/Fe_{10}$ is evidently larger than that of down-spin, leading to the characteristic ferromagnetic exchange splitting with the local magnetic moment of 30.858 μ_B. For $Fe_{10}Au/Au$, the distributions of the up- and down-spin d electrons are nearly equal, resulting in lower spin polarization. So the local magnetic moment of Au in $Fe_{10}Au$ clusters is only 0.142 μ_B. This further confirms that the Fe atomic magnetism is the main contribution to the $Fe_{10}Au$ cluster magnetic moment.

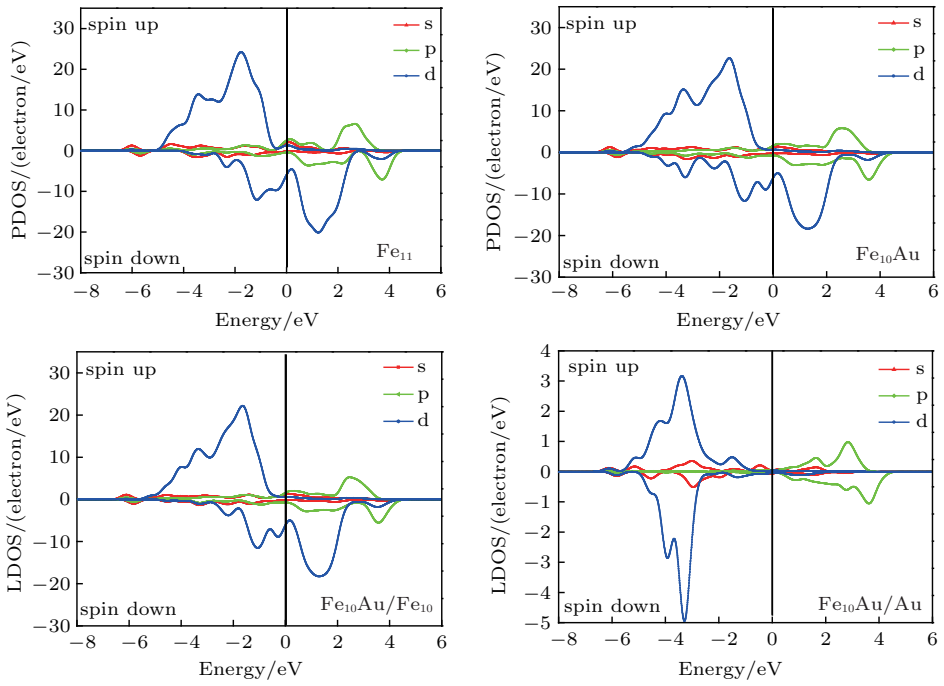


Fig. 9. (color online) PDOSs and LDOSs of $Fe_{10}Au$ and Fe_{11} clusters.

4. Conclusions

In this work, we perform DFT–GGA computations of Fe_nAu (n = 1–12) alloy clusters. The size-dependent structural, electronic, magnetic properties are investigated. The main conclusions are summarized as follows.

(I) The most stable Fe_nAu (n = 1, 2, 4–5, 10–12) clusters can be regared as the structure with Au-substituted surface atom of Fe_{n+1} clusters which keep the similar frameworks to the pure Fe_{n+1} clusters. And the way of growing Fe_nAu (n = 6–9) clusters is that a doping-Au atom occupies a peripheral position of Fe_n clusters.

(II) The calculated fragmentation energy and the second-order difference energy of the Fe_nAu clusters display the similar tendency with clusters size increasing. Of all of the most stable Fe_nAu clusters, Fe_6Au and Fe_9Au possess the highest stabilities. Additionally, both δ_1 and δ_2 are positive for all Fe_nAu clusters, which imply the magnetic stability.

(III) The analysis of atomic net charge Q indicates that the charge always transfers from Fe to Au atom, resulting in the Au atom nearly non-magnetic.

(IV) Magnetism analysis shows that Fe is ferromagnetically coupled with other Fe atoms in these clusters and the doped Au atom exhibits almost no magnetism. The total magnetic moment for most of Fe_nAu clusters is reduced by 3 μ_B

when substituting a Fe atom with an Au atom (except$n = 3$, 11, and 12). This is attributed to the charge transfer between the Fe and Au atoms that causes the Au atom to be nearly non-magnetic, and the doped Au atom has no effect on the average magnetic moment of Fe atoms in Fe_nAu clusters.

Appendix A: Supplementary materials

Supplementary data associated with this article can be found, in the online version, at the following link address: http://cpb.iphy.ac.cn/UserFiles/File/2016-6-063103-Suppl%20Mater.pdf

References

[1] Montano P A and Shenoy G K 1980 *Solid State Commun.* **35** 53
[2] Purdum H, Montano P A, Shenoy G K and Morrison T 1982 *Phys. Rev. B* **25** 4412
[3] Rohlfing E A, Cox D M, Kaldor A and Johnson K H 1984 *J. Chem. Phys.* **81** 3846
[4] Cox D M, Trevor D J, Whetten R L, Rohlfing E A and Kaldor A 1985 *Phys. Rev. B* **32** 7290
[5] Sakurai M, Watanabe K, Sumiyama K and Suzuki K 1999 *J. Chem. Phys.* **111** 235
[6] Cheng Z D, Ling T and Zhu J 2010 *Chin. Phys. B* **19** 057101
[7] Rollmann G, Entel P and Sahoo S 2006 *Comput. Mater. Sci.* **35** 275
[8] Diéguez O, Alemany M M G, Rey C, Ordejón P and Gallego L J 2001 *Phys. Rev. B* **63** 205407
[9] Gutsev G L and Bauschlicher C W 2003 *J. Phys. Chem. A* **107** 7013
[10] Yu S, Chen S, Zhang W, Yu L and Yin Y 2007 *Chem. Phys. Lett.* **446** 217
[11] Ma Q M, Xie Z, Wang J, Liu Y and Li Y C 2007 *Solid State Commun.* **142** 114
[12] Gutsev G L, Weatherford C A, Jena P, Johnson E and Ramachandran B R 2012 *J. Phys. Chem. A* **116** 10218
[13] Kim E, Mohrland A, Weck P F, Pang T, Czerwinski K R and Tománek D 2014 *Chem. Phys. Lett.* **613** 59
[14] Yuan H K, Chen H, Kuang A L, Tian C L and Wang J Z 2013 *J. Chem. Phys.* **139** 034314
[15] Whetten R L, Cox D M, Trevor D J and Kaldor A 1985 *Phys. Rev. Lett.* **54** 1494
[16] Schnabel P and Irion M P 1992 *Ber. Bunsenges Phys. Chem.* **96** 1101
[17] Griffin J B and Armentrout P B 1997 *J. Chem. Phys.* **106** 4448
[18] Lian L, Su C X and Armentrout P B 1992 *J. Chem. Phys.* **97** 4072
[19] Schnabel P, Irion M P and Weil K G 1991 *J. Phys. Chem.* **95** 9688
[20] Schnabel P, Weil K G and Irion M P 1992 *Angew. Chem. Int. Ed. Engl.* **31** 636
[21] Gehret O and Irion M P 1996 *Chem. Phys. Lett.* **254** 379
[22] McCarthy J R and Weissleder R 2008 *Adv. Drug Deliv. Rev.* **60** 1241
[23] Mornet S, Vasseur S, Grasset F and Duguet E 2004 *J. Mater. Chem.* **14** 2161
[24] Laurent S, Forge D, Port M, Roch A, Robic C, Elst L V and Muller R N 2008 *Chem. Rev.* **108** 2064
[25] De H S, Krishnamurty S and Pal S 2010 *J. Phys. Chem. C* **114** 6690
[26] Baishya S and Deka R C 2012 *Comput. Theor. Chem.* **1002** 1
[27] Manzoor D, Pal S and Krishnamurty S 2013 *J. Phys. Chem. C* **117** 20982
[28] Corti C W, Holliday R J and Thompson D T 2005 *Appl. Catal., A Gen.* **291** 253
[29] Service R F 2004 *Science* **306** 2035
[30] Sun Q, Wang Q, Rao B K and Jena P 2004 *Phys. Rev. Lett.* **93** 186803
[31] Wang Y J, Wang C Y and Wang S Y 2011 *Chin. Phys. B* **20** 036801
[32] Liu H L, Hou P, Zhang W X, Kim Y K and Wu J H 2010 *Nanotechnology* **21** 335602
[33] Sun Q, Kandalam A K, Wang Q, Jena P, Kawazoe Y and Marquez M 2006 *Phys. Rev. B* **73** 134409
[34] Wijaya A, Brown K A, Alper J D and Hamad-Schifferli K 2007 *J. Magn. Magn. Mater.* **309** 15
[35] Gorshunov B, Kaiser S, Zhukova E S, Prokhorov A S, Hesselberth M B S, Aarts J, Nieuwenhuys G J and Dressel M 2009 *Phys. Rev. B* **79** 054203
[36] Wilhelm F, Poulopoulos P, Kapaklis V, Kappler J P, Jaouen N, Rogalev A, Yaresko A N and Politis C 2008 *Phys. Rev. B* **77** 224414
[37] Crespo P, Garcìa M A, Pinel E F, Multigner M, Alcántara D, Fuente J M, Penadés S and Hernando A 2006 *Phys. Rev. Lett.* **97** 177203
[38] Sternik M and Parlinski K 2007 *Phys. Rev. B* **75** 212406
[39] Die D, Kuang X Y, Guo J J and Zheng B X 2009 *J. Mol. Struc: Theochem.* **902** 54
[40] Zhang M, He L M, Zhao L X, Feng X J and Luo Y H 2009 *J. Phys. Chem. C* **113** 6491
[41] Torres M B 2005 *Phys. Rev. B* **71** 155412
[42] Yang A, Fa W and Dong J M 2010 *J. Phys. Chem. A* **114** 4031
[43] Wang L M, Bai J, Lechtken A, Huang W, Schooss D, Kappes M M, Zeng X C and Wang L S 2009 *Phys. Rev. B* **79** 033413
[44] Die D, Kuang X Y, Zhu B and Guo J J 2011 *Physica B* **406** 3160
[45] Die D, Kuang X Y, Guo J J and Zheng B X 2010 *Physica A* **389** 5216
[46] Tanaka H, Neukermans S, Janssens E, Silverans R E and Lievens P 2003 *J. Chem. Phys.* **119** 7115
[47] Wang Q, Sun Q, Jena P and Kawazoe Y 2010 *Phys. Chem. Chem. Phys.* **12** 1493
[48] Delley B 1990 *J. Chem. Phys.* **92** 508
[49] Delley B 2000 *J. Chem. Phys.* **113** 7756
[50] Perdew J P, Burke K and Ernzerhof M 1996 *Phys. Rev. Lett.* **77** 3865
[51] Delley B 1998 *Int. J. Quantum Chem.* **69** 423
[52] Song W, Lu W C, Wang C Z and Ho K M 2011 *Comput. Theor. Chem.* **978** 41
[53] Datta S, Kabir M, Ganguly S, Sanyal B, Saha-Dasgupta T and Mookerjee A 2007 *Phys. Rev. B* **76** 014429
[54] Kabir M and Mookerjee A 2006 *Phys. Rev. B* **73** 224439
[55] Wang J L 2007 *Phys. Rev. B* **75** 155422
[56] Shen N F, Wang J L and L Y Zhu 2008 *Chem. Phys. Lett.* **467** 114
[57] Wu P, Yuan L F and Yang J L 2008 *J. Phys. Chem. A* **112** 12320
[58] Tian F Y, Jing Q and Wang Y X 2008 *Phys. Rev. A* **77** 013202
[59] Wang B R, Ma Q M, Liu Y and Li Y C 2009 *Solid State Comm.* **149** 210
[60] Ma Q M, Xie Z, Wang B R, Liu Y and Li Y C 2011 *Solid State Comm.* **151** 806
[61] Liang R R, Lv J and Wu H S 2014 *Eur. Phys. J. D* **68** 187
[62] Aghajani M, Hashemifar S J and Akbarzadeh H 2014 *Physica E* **62** 64
[63] Zhang Y, Duan Y N, Zhang J M and Xu K W 2011 *J. Magn. Magn. Mater.* **323** 842
[64] Chittari B L and Kumar V 2015 *Phys. Rev. B* **92** 125442
[65] Zhao G F, Zhang J and Jing Q 2007 *J. Chem. Phys.* **127** 234312
[66] Lv J, Wang Y C, Zhu L and Ma Y M 2012 *J. Chem. Phys.* **137** 084104
[67] Zhang M, Zhang H, Zhao L, Li Y and Luo Y 2012 *J. Phys. Chem. A* **116** 1493
[68] Weast R C 1974 *CRC Handbook of Chemistry and Physics* (Cleveland: CRC Press)
[69] Ho J, Ervin K M and Lineberger W C 1990 *J. Chem. Phys.* **93** 6987
[70] Brucat P J, Zheng L S, Pettiette C L, Yang S and Smalley R E 1986 *J. Chem. Phys.* **84** 3078
[71] Moskowits M and DiLella D P 1980 *J. Chem. Phys.* **73** 4917
[72] Ferrando R, Jellinek J and Johnston R L 2008 *Chem. Rev.* **108** 845
[73] Lu Q L, Zhu L Z, Ma L and Wang G H 2005 *Chem. Phys. Lett.* **407** 176
[74] Wang J L, Wang G H, Chen X S, Lu W and Zhao J J 2002 *Phys. Rev. B* **66** 014419
[75] Vitos L, Ruban A V, Skriver H L and Kollár J 1998 *Surf. Sci.* **411** 186
[76] Kittel C 2005 *Introduction to Solid State Physics*, 8th edn. (New York: Wiley)
[77] Wang M, Huang X, Du Z and Li Y 2009 *Chem. Phys. Lett.* **480** 258
[78] Zope R R and Baruah T 2001 *Phys. Rev. A* **64** 53202
[79] Li S F and Gong X G 2006 *Phys. Rev. B* **74** 045432
[80] Wang X, Cao Z X, Lu X, Lin M H and Zhang Q E 2005 *J. Chem. Phys.* **123** 064315
[81] Lv J, Zhang F Q, Xu X H and Wu H S 2009 *Chem. Phys.* **363** 65
[82] Venkataramanan N S, Sahara R, Mizuseki H and Y Kawazoe 2010 *J. Phys. Chem. A* **114** 5049
[83] Alonso J A 2000 *Chem. Rev.* **100** 637
[84] Yuan H K, H Chen, Kuang A L, Ahmed A S and Xiong Z H 2007 *Phys. Rev. B* **75** 174412
[85] Zhang G W, Feng Y P and Ong C K 1996 *Z. Phys. D* **38** 241
[86] Duan H M and Zheng Q Q 2001 *Phys. Lett. A* **280** 333